Eur. Phys. J. Plus (2019) **134**: 603
DOI 10.1140/epjp/i2019-13015-3

THE EUROPEAN PHYSICAL JOURNAL PLUS

Regular Article

Design of an accelerator-driven subcritical dual fluid reactor for transmutation of actinides*

Sang-in Bak[1,2], Seung-Woo Hong[3,a], and Yacine Kadi[4]

[1] Korea Institute of Nuclear Safety, Daejeon 34142, Korea
[2] Department of Energy Science, Sungkyunkwan University, Suwon 16419, Korea
[3] Department of Physics, Sungkyunkwan University, Suwon 16419, Korea
[4] European Organization for Nuclear Research (CERN), CH-1211 Geneva, Switzerland

Received: 10 May 2019 / Revised: 4 August 2019
Published online: 5 December 2019

Abstract. An accelerator-driven subcritical dual fluid reactor (AD-DFR), which is a hybrid core operated by a high power accelerator, is designed for the transmutation of minor actinides. The subcritical core is dual in the sense that a lead-bismuth-eutectic–cooled fast reactor (LFR) is combined with a molten salt reactor (MSR). Thus, the core has two loops: one for the liquid metal coolant and the other for the molten salt fuel. The combination of LFR and MSR can take advantages of both reactor types. A subcritical core allows for loading a high fraction of minor actinides in fuels. An 800 MW_t AD-DFR can transmute minor actinides approximately 120 kg/year with only the maximum beam power of 13 MW.

1 Introduction

The management of spent nuclear fuels (SNF) is an important issue for nuclear energy to be sustainable. Transmutation of radioactive nuclides such as long-lived fission products (LLFP) and minor actinides (MA) is an effective way of reducing the burden of the final disposal of SNF.

An accelerator-driven system (ADS) is a hybrid reactor which combines a high power accelerator with a subcritical reactor, and is an option for reducing LLFP and MA with an enhanced safety. The amount of MA transmuted in a fast reactor can be increased if the fraction of MA in the fuel is higher, but the fraction of MA is limited in critical reactors because MA has a low fraction of delayed neutrons (β_{eff}). In contrast to the critical reactors, ADS which can have a large subcritical margin allows for a large fraction of MA in the fuel [1] and can transmute MA intensively. Furthermore, the subcritical core can be easily shut down by switching off the accelerator.

There are mainly two types of ADS cores which have been studied in the past. One of them is a lead-cooled fast reactor (LFR) core. The Energy Amplifier (EA) developed at CERN is a typical example of an ADS based on an LFR core [2]. After the development of the EA, an eXperimental ADS (XADS) was further developed in the 5th European Framework Program in the early 2000s [3]. Development of the JAEA-proposed 800 MW_t ADS [4], MYRRHA at SCK·CEN [5], and CLEAR at INEST [6] followed with a lead-bismuth eutectic (LBE) as a coolant. Another type of an ADS studied is a molten salt fueled ADS. A molten salt subcritical reactor was proposed in the late 1970s for breeding uranium from thorium [7–9]. A molten salt fueled ADS for transmutation of MA was studied under the Accelerator-Driven Transmutation Technology (ADTT) project at the Los Alamos National Laboratory in the 1990s [10,11]. At the same time, an ADS based on chloride salts (NaCl or $PbCl_2$) was studied at JAEA for burning MA in a project called OMEGA [12,13]. Recently, Texas A&M group proposed accelerator-driven subcritical fission in a molten salt core (ADSMS), which is a grid system with 12 sodium-chloride-fueled subcritical reactors of 70 MW_t each [14].

Both the LFR based ADS and MSR based ADS have their own merits and demerits. Lead coolant does not readily react with air or water, and thus LFR does not need an intermediate loop in the heat exchanger or in the steam generator unlike sodium coolant. Also, an LFR core has a hard neutron spectrum due to the heavy atomic mass of lead. Most of the fission cross sections of MA are higher than the neutron capture cross section at neutron energies

* Focus Point on "Advances in the Physics and Thermohydraulics of Nuclear Reactors" edited by J. Ongena.

[a] e-mail: swhong@skku.ac.kr

above several hundred keV. Thus, MA can be transmuted efficiently in the LFR core. In addition, lead has a low neutron capture cross section, and thus the lead coolant is good for the neutron economy. However, reactivity swing of the LFR core is large if a MA burner with only Transuranic fuels (TRU) operates with a high burnup rate. For example, the burnup of the JAEA-proposed ADS is about 116 GWd/tHM, and the beam power needs to be increased almost twice at the end of cycle (EOC) [4]. For reducing the reactivity swing, implementing a burnable poison material surrounding the fuel pins is one of the options [15], but the cost for fabrication of fuels will increase.

On the other hand, a molten salt fueled ADS has a large negative temperature coefficient due to the density change of the liquid fuel, which leads to a high intrinsic reactor safety. An MSR allows the removal of fission products (FP) from the fuel and a continuous or periodical replenishment of fresh fuel while operating the reactor. The online fuel reprocessing can reduce the reactivity swing. Furthermore, this fuel type is free from cracks or swelling that may appear in solid fuels, and the cost for the fuel fabrication can be reduced because the core is fed with fresh fuels through a reprocessing unit directly. As a fuel for an MSR, either fluoride or chloride is used. Fluorine has a low neutron absorption, but the neutron spectrum is much softer than that of chloride. Chlorine, especially Chlorine-35, has a large neutron capture cross section at neutron energies below $\sim$ keV, and thus the core should be designed to keep fast spectra. The neutron spectrum of a chloride-fueled core can be hardened by adding heavier cation chloride such as $PbCl_2$ [12], but it can produce $PbCl_4$ that has the boiling point of only 50 °C, which can increase the pressure of the core [16].

Recently, a new concept called dual-fluid reactor (DFR) [17] was proposed, by combining a lead fast reactor (LFR) with a molten salt fast reactor (MSR). It is a heterogeneous reactor with a molten salt fuel which flows through fuel pipes cooled by a liquid lead coolant. DFR is expected to allow a high power density in a small core volume because there are two liquid loops consisting of a coolant loop and a fuel loop. The liquid fuel and the coolant loops can be operated at a normal pressure. The liquid lead can generate hard neutron spectra and enhance the neutron economy due to its low neutron absorption cross section. The fuel of DFR was chosen as actinide trichlorides with a very high temperature at around 1000 °C without including any carrier salt such as LiCl or NaCl [17]. Recently, a preliminary study on the design of DFR concept was done by using several Monte Carlo codes [18], in which a 3 GW_t reactor was considered for breeding plutonium, and the breeding ratio was 1.06 with the burnup of 20 GWd/tHM.

The DFR concepts in refs. [17,18] are "critical" reactors for the energy production or the breeding of plutonium. In contrast to these original critical DFR concepts, if a "subcritical" DFR core is designed to be driven by an accelerator, the core can have fuels with a higher fraction of MA. In this work, we designed an accelerator-driven subcritical dual fluid reactor (AD-DFR) with the power of 800 MW_t for the transmutation of MA. The accelerator beam power, the subcriticality related to the reactor safety, and the transmutation of MA are estimated.

2 Assumptions and method

2.1 Assumptions

2.1.1 Geometry

The concept of AD-DFR combines an accelerator with an LFR core and a chloride fueled MSR core. Two liquids (LBE and molten salt) circulate separately in the core as a coolant and a fuel. The geometries of the active core and reflectors are taken from JAEA-proposed 800 MW_t ADS [4], and those of the fuel pipes are taken from the DFR designs [17,18].

The inner radius and the thickness of the fuel tube are 7 and 2 mm, respectively. The fuel pipe is made of HT9 which is a high-Cr martensitic steel. The HT9 steel has a good thermal conductivity and irradiation resistance. The ratio of the fuel pitch between two tubes to the fuel diameter (P/D) is about 1.61, which is bigger than the P/D_{pin} value (1.5) of the JAEA-proposed ADS.

The fuel tubes are arranged hexagonally, and the LBE coolant flows between the fuel tubes. A group of 61 fuel tubes are arranged hexagonally with the pitch of 181.9 mm. The total number of fuel pipes is 11712 and they are arranged in the core as shown in the top of fig. 1. The overall dimensions of the core are shown in the bottom of fig. 1. The structure of the inlet and the outlet for the molten salt (fuels) are taken from the DFR concept [17]. The height of the fuel tube is 80 cm, and the fuel inlet and the outlet tanks, which are 10 cm high each, are located at both ends of the tubes. The inlet and the outlet tanks are connected to the tubes. The active core height is 100 cm and its radius is 141.3 cm including the spallation target region. The radius of the spallation target is 17 cm. The target consists of LBE. The LBE reflector and the stainless steel (SS304L) reflector are located outside the active core, and they are 15 cm thick each. The boron carbide (B_4C) neutron shield is 30 cm thick. The fuel pipes for supplying and extracting molten salt fuels to and from the reprocessing unit are omitted in this study. The inclusion of those pipes was tested, and we found the effects were negligible. The design parameters are summarized in table 1. We set the value of k_{eff} to 0.97, as will be explained in sect. 4, and the ratio of the amount of Pu to that of MA was chosen to satisfy $k_{eff} = 0.97$.

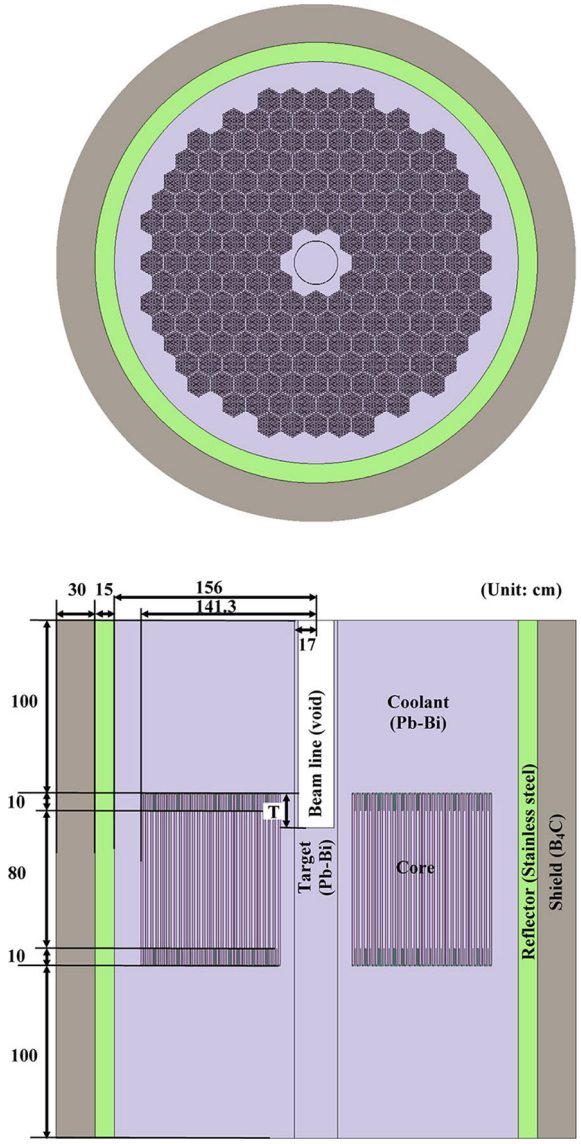

Fig. 1. Schematic diagrams of the AD-DFR considered here.

2.1.2 Molten salt fuel and liquid metal coolant

Molten salt reactors include the carrier salts such as lithium-beryllium fluoride (FLiBe) or NaCl to lower the melting point. In contrast to the typical MSR, the molten salt fuels considered in the DFR studies [17,18] do not include the carrier salts in the primary loop. Therefore, the fuel temperature was kept as high as 1300 K, as it should be higher than the melting point (1040 K) of $PuCl_3$.

Let us consider a fluoride or chloride fuel, and assume that there is no carrier salts such as LiCl and NaCl. MSR is operated at normal pressures, and a high boiling temperature of the fuel is desirable for the safety of a reactor. PuF_3 has the boiling temperature T_B of 2270 K and the melting temperature T_M of 1669 K. It is difficult to find suitable structural materials to sustain at the melting temperature (1669 K) of the fuel. Furthermore, PuF_6 can be produced through the following reaction, $2PuF_3 + 3F_2 \rightleftharpoons 2PuF_6$ [19], and it has very low values of T_M of 325 K and T_B of 335 K, which are too low. Due to the high melting point of PuF_3 and the low boiling point of PuF_6, PuF_3 alone cannot be used as a fuel without including carrier salts.

Likewise, actinide trichlorides also have a limitation to be used as a burner fuel without any carrier salt. $PuCl_3$ has T_M of 1040 K and T_B of 2040 K, and these temperatures are in the range of the DFR concept. However, for transmutation of minor actinides, T_M and T_B of chlorides of minor actinides need to be taken into account. For instance, $AmCl_3$ has T_M of 988 K and T_B of 1120 K. If we have $PuCl_3$ and $AmCl_3$, the fuel temperature should be higher than T_M of 1040 K of $PuCl_3$ and lower than T_B of 1120 K of $AmCl_3$. This means that the temperature of the fuel must be between 1040 K and 1120 K. If the inlet temperature of the fuel is chosen to be 50 K higher than T_M of the

Table 1. AD-DFR specification.

Item	Specification and parameters
Reactor power	800 MW_t
k_{eff}	0.97
Fuel	NaCl+$TRUCl_3$ (66–34 mole %)
Temperature of fuels	874 K
- Pu:MA	53:47 (wt.%)
Coolant	PbBi (44.5–55.5 wt.%)
Total actinide inventory[(a)]	3360 kg
- Pu	1790 kg
- MA	1570 kg
Active core radius[(b)]	141.3 cm
height	100 cm
Fuel tube inner radius	7 mm
Fuel tube thickness	2 mm
Pitch/Fuel diameter	1.61
Total number of fuel pipes	11712
Cycle length	600 EFPD
Reprocess rate	35 liters/day

(a) Initial loaded mass.
(b) Radius including the spallation target region.

fuel, the fuel temperature range available in the core is only 30 K. Boiling of $AmCl_3$ can be prohibited by employing a pressurizer, but then the advantage of the molten salt core for operation at low pressures is lost. Therefore, it is unavoidable for the actinide halides to include a carrier salt to reduce the melting temperature.

Many studies were done in the past on the molten salt fuels based on fluoride salts. The solubility of PuF_3 in the $LiF + BeF_2$ (FLiBe) mixtures was reported to be more or less 1 mole % for $LiF + BeF_2$ and $LiF + BeF_2 + UF_4$ [20–22]. Another fluoride salt such as $LiF + NaF + BeF_2 + PuF_3$ was studied for an actinide burner concept called MOlten Salt Actinide Recycler & Transmuter (MOSART) [23], but the fluoride salt can dissolve PuF_3 only 1.3 mole %. A recent study on the solubility of PuF_3 for LiF + NaF + KF (FLiNaK) measured the solubility to be about 11.1 ± 1.1 mole % at 873 K [24]. In contrast, a chloride mixture can dissolve a large amount of $PuCl_3$. For example, the solubility of $PuCl_3$ for $LiCl + PuCl_3$ and $NaCl + PuCl_3$ is 28 mole % at 734 K and 36 mole % at 726 K, respectively [25].

Although the solubility of PuF_3 for the FLiNaK mixture is higher than that of other fluoride mixtures, the temperature of the FLiNaK based fuel is roughly 100 K higher than that of $LiCl + PuCl_3$ or $NaCl + PuCl_3$. Thus, we selected the $NaCl + PuCl_3$ (66–34 mole %) mixture for AD-DFR to take advantage of high Pu solubility at lower temperatures. The solubility of $AmCl_3$, $NpCl_3$, and $CmCl_3$ need to be investigated further. The solubility of minor actinide trichlorides in NaCl is assumed to be similar to that of $PuCl_3$.

For the density of NaCl+$PuCl_3$, a theoretical study was done for the concept of ADSMS [26]. We took the densities from that study and interpolated the densities as a linear function of temperature for the mixture $NaCl + PuCl_3$ (66–34 mole %)

$$\rho_{(\mathrm{NaCl\text{-}PuCl_3})}\ (\mathrm{g/cm^3}) = 4.0738\text{–}8.4388 \times 10^{-4} T, \tag{1}$$

where T is the temperature in units of K.

The composition of MA and Pu is taken from the SNF of 1 GW_e LWR after 45 GWd/tHM burnup and 20 years' cooling [27]. The detailed composition is shown in table 2. For the purpose of non-proliferation, the extraction of plutonium alone must be excluded from the reprocessing of SNF. However, the fraction of Pu in the whole TRU from SNF is as high as about 84 wt.% [27], and the core is easy to reach the critical state even with a small volume. Thus, we treat the fraction of Pu as a variable parameter to keep the core subcritical.

The MA burner fueled with molten salts can replenish the fresh fuel and remove the FP continuously. The online-reprocessing is one of the advantages of MSR, and it can suppress the reactivity swing during the reactor operation. We take the reprocessing rate of REBUS-3700 concept [28] which assumes that the fission product gases are immediately removed from the core and other FP's are removed by 35 liters of liquid fuel per day.

Table 2. The composition of TRU isotopes used in this work taken from ref. [27]. The weight percentages of Pu and MA add up to 100%, respectively.

Isotope	wt.%	Isotope	wt.%
^{238}Pu	2.53E+0	^{237}Np	4.47E+1
^{239}Pu	6.14E+1	^{241}Am	4.71E+1
^{240}Pu	2.59E+1	^{243}Am	6.86E+0
^{241}Pu	5.12E+0	^{242}Cm	2.45E-4
^{242}Pu	5.05E+0	^{243}Cm	1.82E-2
		^{244}Cm	1.24E+0
		^{245}Cm	1.23E-1
		^{246}Cm	1.51E-2

The liquid coolant for our AD-DFR is chosen as an LBE which was considered for several ADS concepts such as JAEA-proposed ADS [4], and XADS [3,5]. LBE has a low T_M of 397 K while pure lead has T_M of 600 K. T_B of LBE is 1943 K, and LBE cooled reactors do not need to pressurize the reactor even at high temperatures. The density of the LBE coolant as a function of temperature in the range of $400 \leq T \leq 1300$ K is given as [29],

$$\rho_{(\mathrm{LBE})}\ (\mathrm{g/cm^3}) = 11.096\text{–}1.3236 \times 10^{-4} T\ (\mathrm{K}). \tag{2}$$

2.2 Method: Combination of PHITS with SERPENT2

SERPENT2 [30] is a 3-dimensional Monte Carlo transport code and is developed by VTT Technical Research Center of Finland. SERPENT2 (version 2.1.27) was used for the burnup calculations in this work. The value of k_{eff} of our AD-DFR was calculated with the k-eigenvalue criticality source method, and the Chebyshev Rational Approximation Method (CRAM) [31] was used for solving Bateman equations for the fuel depletion. The reprocessing of the fuel was treated by using the mass flow function of SERPENT2. The maximum neutron energy applicable in SERPENT2 is 20 MeV which is the highest neutron energy of the nuclear reaction data file (ENDF), because ENDF/b-VII.0 [32] is used as the nuclear data library. SERPENT2 cannot generate proton beams and the resulting secondary particles. Thus, we divided the whole calculations into two steps by incorporating PHITS [33] with SERPENT2.

PHITS, a particle and heavy ion transport code developed under collaboration between JAEA and other institutes, was used for the calculations of the incident protons, secondary alphas, deuterons, tritons, etc. In generating the secondary particles, Liège Intra-Nuclear Cascade (INCL) model was used in PHITS [34]. The neutrons of energies above 20 MeV were treated by PHITS for further transport calculations. When neutrons of energies less than 20 MeV are generated, the neutrons are recorded and terminated so that they can be used for further calculations by the SERPENT2.

A python program was developed to combine the PHITS for spallation calculations and the SERPENT2 for the reactor core and burnup calculations. The scheme of the computation flows is shown in fig. 2. The PHITS calculation was performed for the spallation reactions and the neutron transports until the neutron energy becomes 20 MeV. The PHITS creates a neutron history file that contains information such as position, direction, energy and time when the energy of a neutron becomes lower than 20 MeV. Then, the python program converts the neutron history file to an external neutron source file for SERPENT2, which does the burn-up calculation by using that source file. After running SERPENT2, the python program checks the depletion of the fuel and updates the depleted fuel material for the next PHITS calculation. The PHITS and the SERPENT2 calculations are repeated automatically until the end of the burnup cycles. In a sense this two-step process of performing the Monte Carlo burnup calculations is similar to the calculations done for the Energy Amplifier study [2] by using FLUKA and EAMC [35]. The limit of the current method is that the depletion of the fuel due to burnup cannot be calculated for the neutron energies above 20 MeV and for particles other than the neutron.

The calculation of the fuel reprocessing was performed by using the mass flow function of SERPENT2. However, the hydrodynamic treatment for the liquid fuel and the coolant is not included and the calculations are based on the steady state. The temperatures of the materials are assumed to be homogeneous and fixed. We assumed the temperature of the fuel to be 874 K which is approximately 100 K higher than the melting temperature T_M of the fuel, and the temperatures of other components are assumed as 824 K for the fuel tube and 774 K for the LBE coolant and other parts.

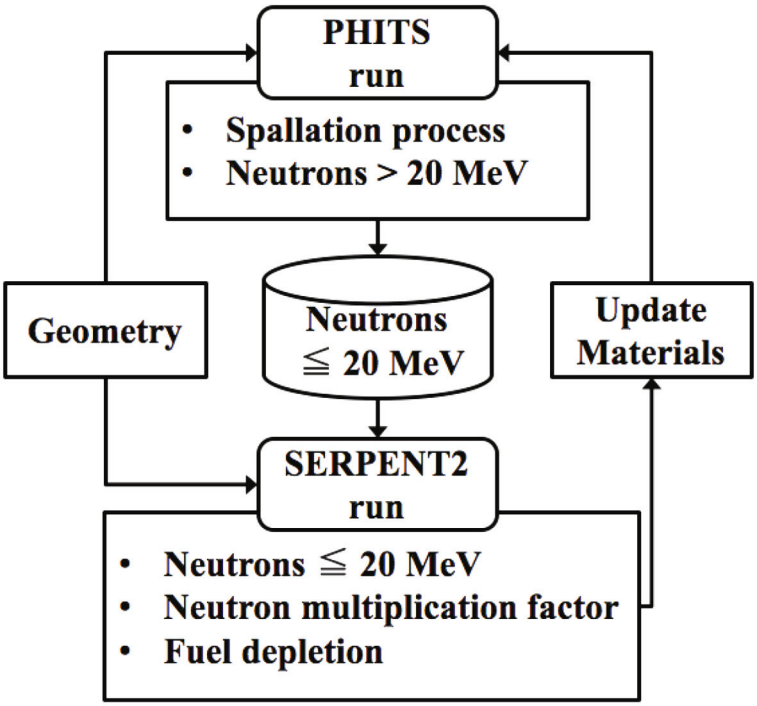

Fig. 2. Coupling scheme of PHITS and SERPENT2 calculations.

The k-eigenvalue criticality source mode calculations for finding the neutron multiplication factor k_{eff} were performed for 1000 cycles with the first hundred cycles inactive. 64000 neutrons were generated for each cycle. The 1-sigma standard deviation of k_{eff} is less than 9×10^{-5} for all the criticality calculations. The external source mode calculations were performed with 3×10^5 neutrons in each cycle as recorded by the PHITS. For the proton beam generation in PHITS simulations, the number of incident protons per batch was 10^4, and a total of 5 batches was made with different random seeds.

3 Optimization of external source

In the design of an ADS, minimization of the accelerator beam power is one of the parameters to be optimized. In general, the spallation target should be able to accommodate high power deposit and to withstand radiation damage. Especially, the high power load and the resulting thermal stress in the beam window restrict the window thickness and the peak power of the beam. Furthermore, minimization of the beam power can reduce a burden on the accelerators.

In view of the reactor core, the beam power can be minimized by enhancing the source efficiency, and the source efficiency can be increased if the target and the core design are improved [36,37]. The accelerator beam power P_{acc} (in W) for achieving a given thermal power P (in W) of the reactor can be expressed by

$$P_{acc} = \frac{P}{(\bar{f}_n/\bar{n})\bar{E}_f} \frac{1}{(\bar{n}/\bar{p})} E_p. \tag{3}$$

Herein, $\bar{f}_n/\bar{n}$ stands for the average total number of fissions per a source neutron, $\bar{E}_f$ is the average recoverable energy (in eV) per fission, $\bar{n}/\bar{p}$ is the average spallation neutrons generated per incident proton, and E_p is the incident proton energy (in eV). The factor $\frac{P}{(\bar{f}_n/\bar{n})\bar{E}_f}$ can be calculated by SERPENT2 when the external source mode is used, while the value of $\bar{n}/\bar{p}$ is provided by PHITS.

To optimize the beam power and the position of the beam pipe (beam window), the required beam power, P_{acc}, for 800 MW_t core was calculated for different proton energies and different target positions by changing the distance from the top of the core to the beam window. As is shown in fig. 1, the LBE target for spallation is physically separated from the LBE coolant by installing a stainless steel wall. The radius of the spallation target and the buffer region together was fixed as 20 cm. The proton beam distribution in space was assumed as a Gaussian distribution with FWHM of 2 cm. The proton energy was varied from 600 MeV to 1.5 GeV. Higher energies are not needed for AD-DFR because the projected range of protons of higher energies in LBE will overshoot the active core area of which the length is chosen as 1 m. The projected range for 1.5 GeV proton in LBE is approxiamtely 1 m [38].

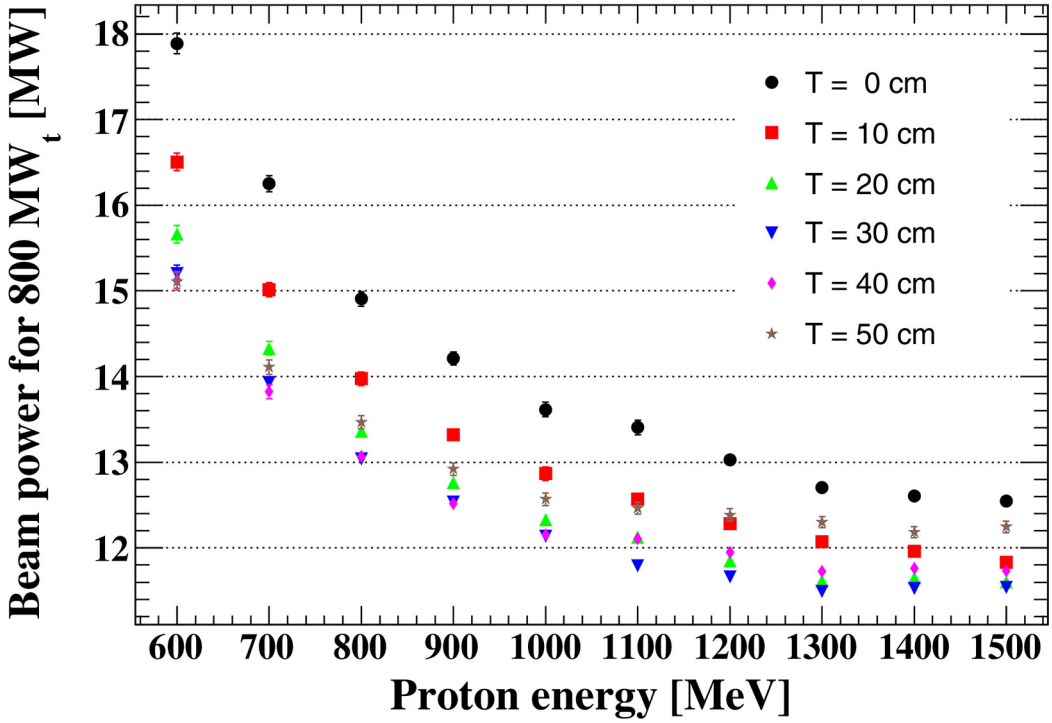

Fig. 3. Accelerator beam power P_{acc} required for an 800 MW_t reactor is plotted as a function of the proton energy for different values of T, which is the distance from the top of the core to the beam window as shown in fig. 1 (max. error ~ 0.12 MW).

Figure 3 shows the required P_{acc} for 800 MW_t reactor power as a function of proton energies. Different symbols denote the required P_{acc} for each target position. The minimum value of P_{acc} is around 11.6 MW, when the proton energy is 1.3–1.5 GeV and the beam pipe is located 20–30 cm below the top of the core. We thus selected for the preceding calculations the proton energy of 1.5 GeV and the target position of $T = 20$ cm. The incident proton beam current required is 7.74 ± 0.04 mA. The rest of the calculations are carried out with these parameters.

4 Determination of subcriticality margin

Generally, an ADS with a higher value of k_{eff} requires a lower beam power than that with a lower k_{eff}. However, subcriticality needs to be kept sufficiently below some limit for safety reasons. The reactor should be in a subcritical state in the operational condition, in the fuel loading condition, and in any accidental condition. There were studies on determining the subcriticality of ADS [4,39]. The k_{eff} of a subcritical reactor should satisfy the following relation in any reactor condition:

$$k_{eff} + \delta k_{eff}^{TD} + \delta k_{eff}^{AC} + \delta k_{eff}^{UM} + \delta k_{eff}^{UC} < 1, \tag{4}$$

where δk_{eff}^{TD} is the reactivity increase caused by temperature swing from the full power state to a cold refueling state, and δk_{eff}^{AC} is the reactivity insertion by accidental conditions. δk_{eff}^{UM} and δk_{eff}^{UC} refer to the uncertainties associated with the reactivity measurement and calculation, respectively.

The reactivity insertion by the temperature swing, δk_{eff}^{TD}, can be estimated from the temperature coefficients. There are two different liquid materials in the AD-DFR core: the coolant and the molten salt fuel. For the reactor safety, the temperatures of the coolant and the fuel must be sufficiently higher than the freezing temperatures in the refueling condition. In this work, the refueling temperatures of the fuel and the coolant are assumed as 776 K and 447 K, respectively, which are about 50 K higher than the melting (and eutectic) temperatures.

Although there can be various accidental conditions, δk_{eff}^{AC} is estimated by considering two accidental conditions; the failure of the beam window and the unusual temperature increases. The failure of the beam window would cause the LBE coolant to flow into the beam pipe, and the loss of fission neutrons through the beam pipe would decrease. Thus, the beam window failure leads to an increase in the reactivity of the reactor. In estimating the reactivity change, it is assumed that the coolant would fill in the beam pipe without including other changes such as temperatures, densities, etc.

Significant changes in the temperature of the coolant and the fuel, which can be caused for some accidental reason, may lead to the reactivity changes. We assumed the temperature of the coolant and the fuel increases up to 1273 K (1000 °C) and calculated the reactivity changes as follows.

Table 3. Estimated reactivity swing for different considerations and the estimated maximum Δk_{eff}.

Considered parameters	$\times 10^2\ \Delta k/k$
δk_{eff}^{TD}	
- System cool-down to cold refueling point	1.185 ± 0.012
δk_{eff}^{AC}	
- Beam pipe filled with the coolant	0.144 ± 0.013
- Increase in coolant temperature[(a)]	-0.339 ± 0.018
- Increase in fuel temperature[(a)]	-4.789 ± 0.017
δk_{eff}^{UM}	
- Uncertainties in measurements	0.300
δk_{eff}^{UC}	
- Uncertainties in calculations	1.000
Total $(\delta k_{eff}^{TD} + \delta k_{eff}^{AC} + \delta k_{eff}^{UM} + \delta k_{eff}^{UC})$[(b)]	2.630 ± 0.017
k_{eff}	0.9737 ± 0.0002

[(a)] Temperature is assumed to increase to 1273 K.
[(b)] Sum of the positive values.

The reactivity swing under the conditions mentioned above is estimated by using the following equation:

$$\Delta\rho\,(\Delta k/k) = \frac{1}{k_{eff}} - \frac{1}{k'_{eff}}\,, \tag{5}$$

where k_{eff} is the neutron multiplication factor in full power operation, and k'_{eff} is that under different conditions. We estimated k_{eff} from the k_{eff} at the beginning of cycle (BOC). δk_{eff}^{AC} was calculated as the sum of $\delta k_{eff}^{AC}|_{Doppler}$ and $\delta k_{eff}^{AC}|_{Density}$ due to an accidental temperature increase.

The uncertainties in the reactivity, δk_{eff}^{UC} and δk_{eff}^{UM}, are assumed roughly to be 1% $\Delta k/k$ in the calculation and 10% in the measurement of the subcriticality [4]. We take the subcriticality of the core equal 3% $\Delta k/k$ for $k_{eff} = 0.97$. Then the uncertainty in the measurement of the subcriticality becomes 0.3% $\Delta k/k$.

Table 3 shows the estimated reactivity swing under different conditions and the estimated k_{eff}. We found that when the temperature of the fuel increases the reactivity decreases significantly due to the large negative temperature feedback of the liquid fuel. This behavior is the advantage of the liquid fuel. On the other hand, the reactivity increases when the core is under the refueling condition, because of the increase in the fuel density at lower temperatures. Given the total reactivity change as discussed above, $k_{eff} = 0.97$ seems acceptable as the initial condition. The upper limit of k_{eff} of the system is about 0.973.

In addition, if the core loses all the LBE coolant, k_{eff} becomes 0.68 which means there is a significant negative reactivity insertion in the accidental condition like loss of the coolant accident (LOCA). Other accidental considerations such as the leakage of the liquid fuel into the coolant is out of the scope of the present work and is left for a future work.

5 Neutron spectrum of AD-DFR

The normalized spectrum of the source neutrons produced by the incident proton beam is calculated by the PHITS and is shown in fig. 4 by the black dotted line. The peak of the spectrum is located at around 2–3 MeV, and the neutrons of energy greater than 20 MeV are approximately 16.6% of the entire source neutrons. The red solid line in fig. 4 is the neutron spectrum in the molten salt fuel region of the AD-DFR core. About 53% of neutrons are in the energy range between 0.1 and 1 MeV, and the neutrons with energies above 20 MeV are less than 0.01% of the neutrons. It means the spallation source neutrons lose most of their energies or generate other particles through nonelastic scatterings in the LBE coolant region. Although our calculation method of combing PHITS and SERPENT2 has a limit in the burnup calculation in the sense that neutrons with energies greater than 20 MeV are not included in the burnup calculation, the fraction of the neutrons above 20 MeV is only 0.01% and may not have a significant effect on the calculation of the fuel depletion.

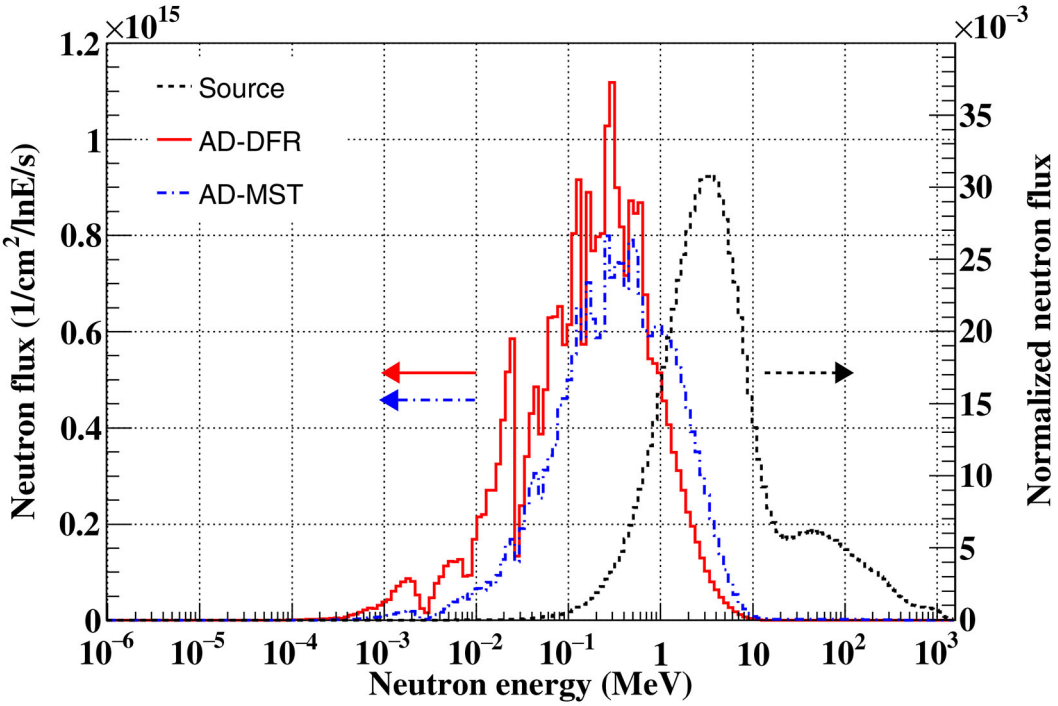

Fig. 4. Normalized spectra of source neutrons produced by the proton beam of 1.5 GeV are plotted by the black dotted line. The vertical axis on the right-hand side is for these source neutrons. Normalized neutron spectra in the molten salt fuel region in the AD-DFR are plotted by the red solid line, and those in the fuel region of AD-MST [12] are plotted by the blue dot-dashed line. The vertical axis on the left-hand side is for these two neutron spectra.

To compare our results with a previous work, we performed calculations on an accelerator-driven molten salt target (AD-MST) system based on the JAEA model [12,13]. The molten salt fuel of AD-MST is NaCl-TRUCl_3 (66–34 mole %) just like the fuel of AD-DFR, but the ratio between Pu and TRU is different from AD-DFR. The normalized neutron spectrum of AD-MST is plotted by the blue dot-dashed line in fig. 4. The neutron spectrum of AD-MST is located at higher energies in comparison to the neutron spectrum of AD-DFR. These spectra indicate that the LBE coolant of AD-DFR cannot improve the neutron spectrum for the transmutation of MA. This behavior can be explained by the loss of energies of fission neutrons of AD-DFR while they travel from one fuel tube to other fuel tubes through HT9 tube and LBE coolant. The LBE coolant allows more neutrons survive below approximately 20 keV because the neutron absorption cross section of Pb and Bi is much less than that of ^{35}Cl. Although the neutron spectrum of AD-DFR becomes less effective for the transmutation of MA than that of AD-MST, the presence of the LBE target and the coolant still reduces the beam power. The beam power required for the AD-MST is about 15 MW for 800 MW_t, which is much higher than that (12 MW) for the AD-DFR as shown in fig. 3.

6 Reactivity swing and transmutation of MA

One of the advantages of the molten salt fueled core is that the fuel can be continuously reprocessed and supplied with new fuels. While the value of k_{eff} decreases with time for a solid fueled ADS [4], the online-reprocessing of MSR can reduce the reactivity swing. It means that the molten salt core can suppress the increase of the beam power. We investigated the changes in k_{eff} with time depending on different replenishment of fuels and the resulting transmutation of MA.

We used the CRAM method [31] for the calculations of the fuel depletion and used the mass flow function for reprocessing of the fuel. These are the functions provided by SERPENT2. We assumed the reprocessing rate as follows:

- 99% of the generated gases such as He, Ne, Ar, Kr, Xe, Rn and I [12] are extracted from the core immediately;
- 35 liters of the fuel are reprocessed daily to remove the FP [28]; and
- an average of 0.7 kg of TRU (Pu and MA) per day is replenished into the core.

The length of one cycle was chosen as 600 effective full power days (EFPD), and a total of 10 cycles (6000 EFPD) was calculated. The ratio of Pu and MA in the initial fuel in the core is 53:47 (wt.%), and all FPs are replaced by MA after each cycle.

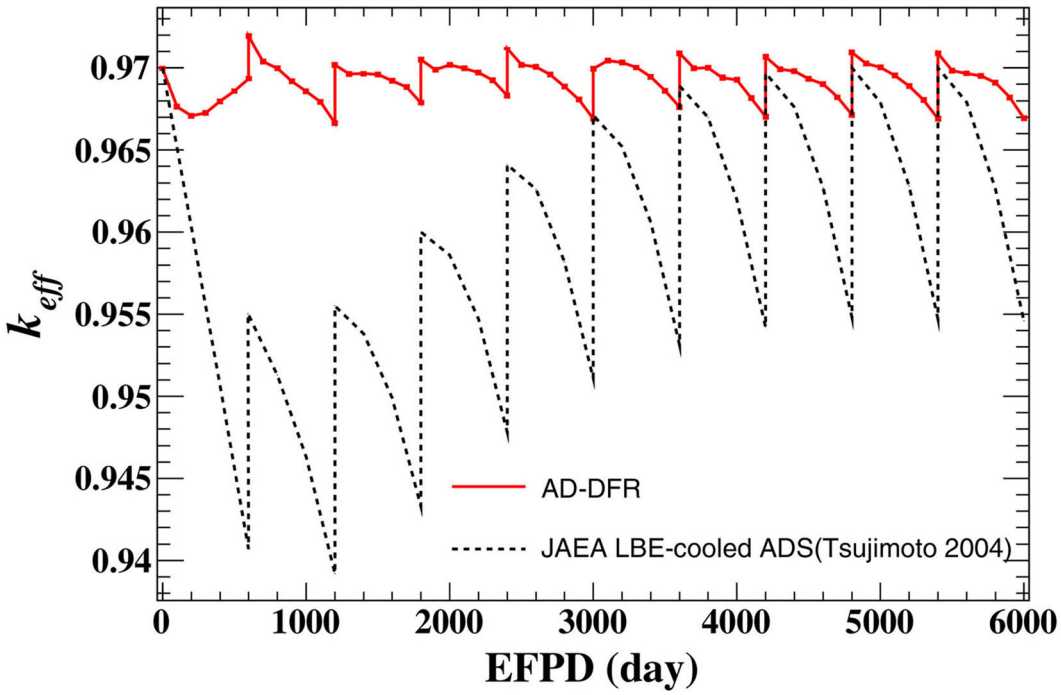

Fig. 5. The effective neutron multiplication factor k_{eff} of AD-DFR with time change, and that of the JAEA-proposed ADS [4] (max. error is 0.00009).

The fraction of Pu in the replenishing fuel is varied from 53 wt.% to 68 wt.%. Although the fuel in the core is continuously reprocessed, FPs remain in the core because only part of the fuel (35 liters/day) is reprocessed over time. If the amount of injected TRU is the same as that of the extracted FP, then the injected TRU is less than the amount of fuels consumed by fissions. Thus the fraction of Pu in the replenishing fuel needs to be changed. In this study, we limited ourselves to the use of fixed ratios of Pu:MA at each cycle for simplicity.

Figure 5 shows the time evolution of the effective neutron multiplication factor k_{eff} of the AD-DFR (red solid line) and that of the JAEA-proposed ADS (black dotted line) which has a solid fuel core [4]. In comparison with the solid-fueled ADS, AD-DFR can efficiently suppress the reactivity swing because of the reprocessing of the fuel. The lowest k_{eff} is 0.967 which corresponds to only $0.3\%\Delta k/k$, and the highest k_{eff} is 0.972.

The maximum required beam current I_B for this AD-DFR is 8.62 ± 0.04 mA during 10 cycles, and this value is just 1 mA higher than the initial beam current. The burnup of AD-DFR is almost 140 GWd/tHM, and this value is very high in comparison with that from the other ADS such as the JAEA-proposed molten salt ADS [12,13], LBE-cooled ADS [4], and ADSMS [14]. Notwithstanding such a high burnup, the beam power can be maintained at sufficiently low values due to the online-reprocessing.

The amount of the transmuted MA after 10 cycles is 2.33 tonnes, and the average transmuted MA is about 117 kg/year. This amounts to the mass of MA annually produced by roughly four 1 GW_e LWRs. The amount of the transmuted MA is about 130 kg/year less than that of the JAEA-proposed ADS (250 kg/year) [4]. The difference is due to the total mass of the loaded MA. The JAEA-proposed ADS loads 2.5 tons of MA, whereas 1.6 tons of the initial MA are loaded for our AD-DFR. The mass of MA decreases with time as shown in fig. 6. The mass of Pu increases up to 2.1 tons, and that of MA decreases from 1.6 to 1.2 tons during 10 cycles. Increasing the fraction of $TRUCl_3$ in the fuel could increase the MA transmutation by choosing the NaCl-$TRUCl_3$ fuel as 50-50 mole % if the fuel temperature is allowed to increase roughly 100 K [25]. However, the physical and chemical properties of such a fuel are not known, and studies of using such a fuel is not doable at the moment.

The advantage of the AD-DFR over the JAEA-proposed ADS is a small reactivity swing despite high burnup rate. It lowers the burden on the accelerator and enhanves safety. However, the transmutation of MA is much less than the JAEA-proposed ADS because of the low initial inventory of MA.

7 Conclusion and discussion

In this work, we proposed an AD-DFR design for an 800 MW_t reactor. AD-DFR is a novel concept which combines an LBE-cooled ADS with an MSR core for transmutation of MA. Although there are still many challenges such as the corrosion of the structural materials by molten salts and LBE coolant at high temperatures, AD-DFR can be a

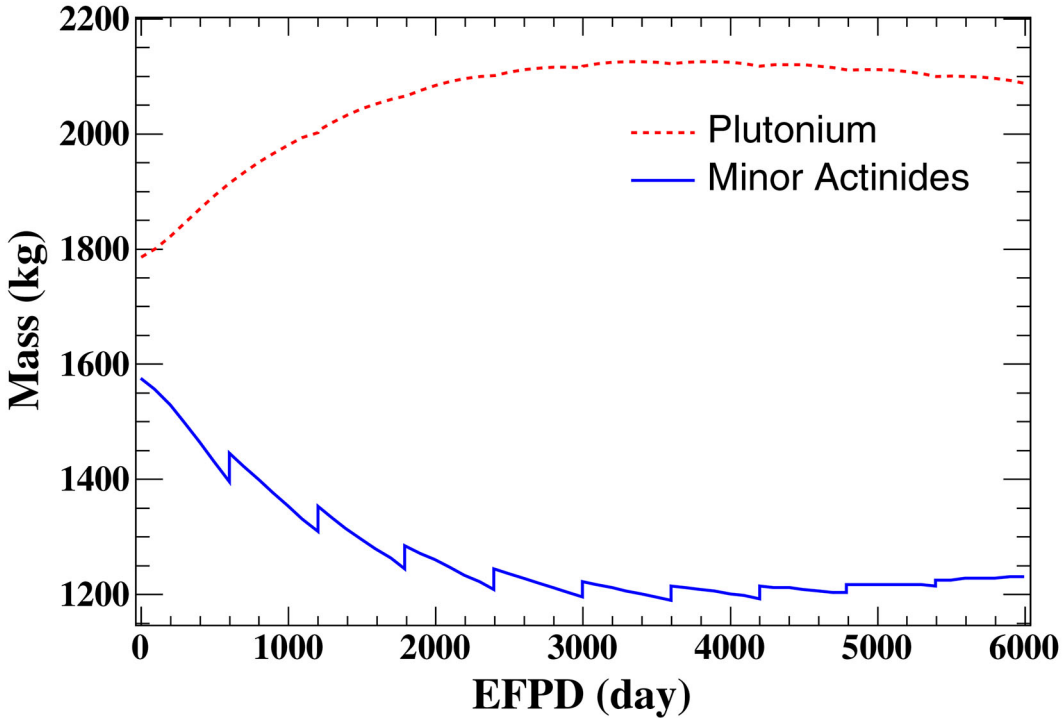

Fig. 6. The mass of Pu and MA in the core with time change.

good option by taking advantages of merits of MSR, LFR, and ADS. AD-DFR has an enhanced intrinsic safety due to a large negative temperature feedback, and a large subcritical margin which allows a high fraction of MA.

Although the neutron spectrum of AD-DFR is shifted to lower energies in comparison with that of AD-MSR, the required beam current of the AD-DFR decreases efficiently. The maximum beam current required is 8.6 mA for 1.5 GeV proton beams for an 800 MW_t reactor, and the reprocessing of the fuel can suppress the reactivity swing sufficiently. The AD-DFR can transmute about 117 kg of MA per year. This amount of transmuted MA is equal to the amount of MA produced by four 1 GW_e LWRs per year. Only Monte Carlo particle transport and burnup calculations are performed in this work without the hydrodynamic calculations. Thus, a hydrodynamic study for such a system needs to be carried out in the future.

We thank Prof. M.H. Kim for his helpful comments. This work was supported in part by the National Research Foundation of Korea (NRF) grant funded by the Korean government (MSIT) (No. NRF-2018M2A8A2083829).

References

1. H. Nifenecker, O. Meplan, S. David, C. R. Acad. Sci. IV **2**, 163 (2001).
2. C. Rubbia, J.A. Rubio, S. Buono, F. Carminati, N. Fiétier, J. Gálvez, C. Gelès, Y. Kadi, R. Klapisch, P. Mandrillon *et al.*, Tech. Rep. AT/95-44 (ET) (CERN, Geneva, 1995).
3. L. Cinotti, B. Giraud, H.A. Abderrahim, J. Nucl. Mater. **335**, 148 (2004).
4. K. Tsujimoto, T. Sasa, K. Nishihara, H. Oigawa, H. Takano, J. Nucl. Sci. Technol. **41**, 21 (2004).
5. H.A. Abderrahim, P. Baeten, D. De Bruyn, R. Fernandez, Energy Convers. Manag. **63**, 4 (2012).
6. Y. Wu, Y. Bai, Y. Song, Q. Huang, Z. Zhao, L. Hu, Ann. Nucl. Energy **87**, 511 (2016).
7. J.S. Fraser, IEEE Trans. Nucl. Sci. **NS-24**, 1611 (1977).
8. K. Tsukada, J. At. Energy Soc. Jpn. **20**, 1 (1978).
9. K. Furukawa, H. Ohno, J. Mochinaga, K. Igarashi, J. Nucl. Sci. Technol. **17**, 562 (1980).
10. C.D. Bowman, E.D. Arthur, P.W. Lisowski, Nucl. Instrum. Methods Phys. Res. Sect. A **320**, 336 (1992).
11. C.D. Bowman, *Basis and objectives of the Los Alamos Accelerator-Driven Transmutation technology project*, in *The International Conference on Accelerator-Driven Transmutation Technologies and Applications* (AIP, 1995) pp. 22–43.

12. Y. Kato, H. Katsuta, T. Takizuka, H. Takada, H. Yoshida, *Accelerator molten salt target system for transmutation of long lived nuclides*, in *Specialists' Meeting on Acceleraotr Based Transmutation (PSI, 24-26 March 1992)* (1992) pp. 133–143.
13. T. Mukaiyama, T. Takizuka, M. Mizumoto, Y. Ikeda, T. Ogawa, A. Hasegawa, H. Takada, H. Takano, Prog. Nucl. Energy **38**, 107 (2001).
14. P. McIntyre, S. Assadi, K. Badgley, W. Baker, J. Comeaux, J. Gerity, J. Kellams, A. McInturff, N. Pogue, S. Phongikaroon *et al.*, *Accelerator-driven subcritical fission in molten salt core: Closing the nuclear fuel cycle for green nuclear energy*, in *Application of Accelerators in Research and Industry: Twenty-Second International Conference* (AIP, 2013) pp. 636–642.
15. N. Aizawa, T. Iwasaki, Y. Watanabe, T. Takani, J. Nucl. Sci. Technol. **53**, 240 (2015).
16. D.E. Holcomb, G.F. Flanagan, B.W. Patton, J.C. Gehin, R.L. Howard, T.J. Harrison, Tech. Rep. ORNL/TM-2011/105 (Oak Ridge National Laboratory, 2011).
17. A. Huke, G. Ruprecht, D. Weißbach, S. Gottlieb, A. Hussein, K. Czerski, Ann. Nucl. Energy **80**, 225 (2015).
18. X. Wang, R. Macian-Juan, M. Seidl, *Preliminary Analysis of Basic Reactor Physics of the Dual Fluid Reactor Concept*, in *International Congress on Advances in Nuclear Power Plants (ICAPP)* (Nice, 2015) p. 11.
19. A.E. Florin, I.R. Tannenbaum, J.F. Lemons, J. Inorg. Nucl. Chem. **2**, 368 (1956).
20. C.J. Barton, J. Phys. Colloid Chem. **64**, 306 (1960).
21. L.M. Ferris, J.C. Mailen, F.J. Smith, J. Chem. Eng. Data **16**, 68 (1971).
22. L.I. Ponomarev, M.B. Seregin, A.P. Parshin, S.A. Mel'nikov, A.A. Mikhalichenko, L.P. Zagorets, R.N. Manuilov, A.A. Rzheutskii, Sov. At. Energy **115**, 5 (2013).
23. V. Ignatiev, O. Feynberg, I. Gnidoi, A. Merzlyakov, *Progress in development of Li, Be, Na/F molten salt actinide recycler & transmuter concept*, in *International Congress on Advances in Nuclear Power Plants (ICAPP)* (2007) p. 10.
24. A.A. Lizin, S.V. Tomilin, O.E. Gnevashov, R.K. Gazizov, A.G. Osipenko, M.V. Kormilitsyn, A.A. Baranov, L.V. Zaharova, V.S. Naumov, L.I. Ponomarev, Sov. At. Energy **115**, 11 (2013).
25. C.W. Bjorklund, J.G. Reavis, J.A. Leary, K.A. Walsh, J. Phys. Chem. **63**, 1774 (1959).
26. E. Sooby, A. Baty, O. Benes, P. McIntyre, N. Pogue, M. Salanne, A. Sattarov, J. Nucl. Mater. **440**, 298 (2013).
27. C.H. Kim, Tech. Rep. 57, Korean Acad. Sci. Technol. (2010).
28. A. Mourogov, P.M. Bokov, Energy Convers. Manag. **47**, 2761 (2006).
29. V. Sobolev, J. Nucl. Mater. **362**, 235 (2007).
30. J. Leppänen, M. Pusa, T. Viitanen, V. Valtavirta, T. Kaltiaisenaho, Ann. Nucl. Energy **82**, 142 (2015).
31. M. Pusa, J. Leppänen, Nucl. Sci. Eng. **164**, 140 (2010).
32. M.B. Chadwick, P. Obložinský, M. Herman, N.M. Greene, R.D. McKnight, D.L. Smith, P.G. Young, R.E. MacFarlane, G.M. Hale, S.C. Frankle *et al.*, Nucl. Data Sheets **107**, 2931 (2006).
33. T. Sato, K. Niita, N. Matsuda, S. Hashimoto, Y. Iwamoto, S. Noda, T. Ogawa, H. Iwase, H. Nakashima, T. Fukahori *et al.*, J. Nucl. Sci. Technol. **50**, 913 (2013).
34. A. Boudard, J. Cugnon, J.C. David, S. Leray, D. Mancusi, Phys. Rev. C **87**, 014606 (2013).
35. Y. Kadi, *Transmutation Potential of the Energy Amplifier Demonstration Facility Calculated with the EA-MC Code Package*, in *Workshop on Hybrid Nuclear Systems for Energy Production, Utilisation of Actnides Si Transmutation of Long-Lived Radioactive Waste* (ICTP, 2001).
36. P. Seltborg, J. Wallenius, K. Tucek, W. Gudowski, Nucl. Sci. Eng. **145**, 390 (2003).
37. S.I. Bak, S.W. Hong, Y. Kadi, J. Nucl. Sci. Technol. **54**, 862 (2017).
38. J.F. Ziegler, M.D. Ziegler, J.P. Biersack, Nucl. Instrum. Methods Phys. Res. B **268**, 1818 (2010).
39. Y. Kim, W. Park, R.N. Hill, *An investigation of subcriticality level in accelerator-driven system*, in *PHYSOR 2002 International Conference on the New Frontiers of Nuclear Technology: Reactor Physics, Safety and High-Performance Computing* (Seoul, Korea, 2002).